Photolysis of Nitric Acid at 308 nm in the Absence and Presence of Water Vapor

ARTICLE *in* THE JOURNAL OF PHYSICAL CHEMISTRY A · APRIL 2015

Impact Factor: 2.69 · DOI: 10.1021/acs.jpca.5b00951 · Source: PubMed

5 AUTHORS, INCLUDING:

Manuvesh Sangwan
Carnegie Institution for Science
15 PUBLICATIONS **46** CITATIONS

THE JOURNAL OF PHYSICAL CHEMISTRY A

Article

pubs.acs.org/JPCA

Photolysis of Nitric Acid at 308 nm in the Absence and in the Presence of Water Vapor

Lei Zhu,* Manuvesh Sangwan, Li Huang,† Juan Du, and Liang T. Chu

Wadsworth Center, New York State Department of Health, Department of Environmental Health Sciences, SUNY-Albany, Albany, New York 12201, United States

ABSTRACT: We have re-examined the NO_x channels from the 308 nm gas-phase photolysis of nitric acid (HNO_3) by using excimer laser photolysis combined with cavity ring-down spectroscopy. The photolysis products were monitored in the 552−560 and 640−648 nm regions. Direct comparison of the photolysis product spectrum in the 640−648 nm region with literature vibronic band origins and line intensities in electronically excited NO_2 (NO_2*) suggests that NO_2* is not formed from HNO_3 photolysis at 308 nm. A comparison of the photolysis product spectrum in the 552−560 nm region with a standard NO_2 spectrum indicates that ground-state NO_2 is a photolysis product. We have determined the NO_2 quantum yield from the 308 nm HNO_3 photolysis. We also investigated HNO_3 photolysis in the presence of water vapor. For equilibrated HNO_3/H_2O mixtures, we did not observe significant variation of product absorption around 552 nm with delay times between the firing of the photolysis and the probe lasers. Transient product absorption measurements at 342.0 and 343.5 nm (respective wavelengths where the peak and valley of HONO absorptions are located) are consistent with ground-state NO_2 being the predominant NO_x product from the 308 nm photolysis of a HNO_3/H_2O mixture. Atmospheric implications are also discussed.

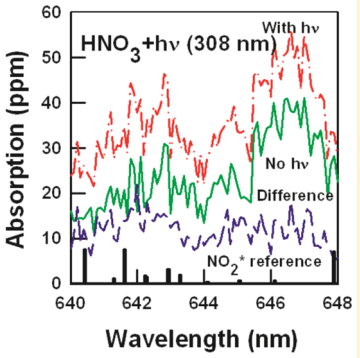

1. INTRODUCTION

Field studies[1,2] have shown that atmospheric daytime HONO levels greatly exceed those calculated on the basis of a photochemical stationary state involving OH, NO, and HONO. Various photochemical HONO formation mechanisms have been proposed to explain such a discrepancy. One proposed HONO source is the sunlight photolysis of nitric acid (HNO_3) adsorbed on ground surfaces.[3−5] Observation of HONO formation after glass manifold surfaces coated with HNO_3 and H_2O are exposed to sunlight appears to support such a hypothesis.[5] Reaction of H_2O with electronically excited NO_2 (NO_2*), generated by sunlight photolysis of adsorbed HNO_3, has been postulated to be the cause of HONO formation (NO_2* + H_2O = HONO + OH).[3] Field experiments monitor only the end-products; a complex mixture of reactants in addition to HNO_3 and water vapor, and complex matrices of surfaces, could play the role of photosensitizers in HONO formation. To experimentally verify whether HONO can be formed from the proposed photolysis of the HNO_3 and H_2O only system by sunlight, as well as whether NO_2* is a HNO_3 photolysis product, we have investigated the 308 nm gas-phase photolysis of HNO_3 in the absence and in the presence of water vapor. Studying gas-phase photolysis of HNO_3 and HNO_3/H_2O mixtures is necessary in order to determine whether HONO formation is energetically feasible following sunlight photolysis of HNO_3 in the presence of water vapor.

Gas-phase photolysis of nitric acid in the actinic UV region ($\lambda \geq 290$ nm) can occur through the following pathways:

$$HNO_3 + h\nu \rightarrow OH + NO_2 \quad (\lambda \leq 604\ \text{nm}) \tag{1}$$

$$\rightarrow OH + NO_2^* \quad (\lambda \leq 381\ \text{nm}) \tag{2}$$

$$\rightarrow HONO + O(^3P) \quad (\lambda \leq 393\ \text{nm}) \tag{3}$$

where photochemical thresholds were calculated from the corresponding enthalpy changes.[6] While the gas-phase photolysis of HNO_3 in the 190−250 nm region has been studied extensively,[7−26] only a few studies[27−29] were conducted around 300 nm. These few photolysis studies mostly monitored the OH product. The OH quantum yield from the photolysis of HNO_3 vapor at 308 nm was determined using a laser-induced fluorescence (LIF) technique.[28] An OH quantum yield of 1.05 ± 0.29 was obtained. August and co-workers[27] used Doppler-resolved LIF to probe the scalar and vector properties of the OH(X) fragments generated from HNO_3 photodissociation at 280 nm. Photodissociation at 280 nm was postulated to occur through a vibronically mediated transition to an electronic state of A″ character. The internal modes of NO_2 contained 70% of the excess energy, and 30% was in the OH and NO_2 translational mode. Thermodynamically, the excess energy following 308 nm photolysis of HNO_3 (eq 1) is estimated to be about 43.8 kcal/mol.[29] Assuming the excess energy is partitioned in a similar fashion for both 308 and 280 nm HNO_3 photolysis, the internal energy of the NO_2 chromophore from 308 nm photolysis can be up to 30.7 kcal/mol. In the visible spectral region,[30,31] the lowest energy vibronic transition for NO_2 is between the electronically excited 1^2B_2 state and the

Received: January 29, 2015
Revised: April 19, 2015
Published: April 24, 2015

DOI: 10.1021/acs.jpca.5b00951
J. Phys. Chem. A 2015, 119, 4907−4914

ground X^2A_1 state. The energy level between these two states is strongly dependent on the geometry of NO_2, in particular the bending angle. The calculated excess internal energy (30.7 kcal/mol) is only slightly higher (about 3 kcal/mol) than the lowest energy[30,31] between X^2A_1 and 1^2B_2. Thus, in principle, a NO_2 chromophore formed from the HNO_3 photolysis at 308 nm could be either NO_2 or NO_2*, or both. We previously conducted the only time-resolved study of the NO_x channel following HNO_3 photolysis at 308 nm; we suggested that OH + NO_2* is a dominant HNO_3 photolysis channel.[29] The nature of the NO_x product(s) formed from the HNO_3 photolysis is important because, if NO_2* is formed from HNO_3 photolysis at 308 nm, it may react with H_2O to form HONO + OH; the proposed mechanism for atmospheric HONO formation from adsorbed HNO_3 photolysis may hold. On the other hand, if the ground-state NO_2 is formed from the 308 nm HNO_3 photolysis, the proposed mechanism for the HONO formation from sunlight photolysis of nitric acid in the presence of H_2O may not hold. Given that there is only one published time-resolved study on the NO_x production channel from HNO_3 photolysis in the actinic UV region,[29] and in light of some of our recent laboratory work, there is uncertainty in the nature of the electronic states of NO_2 in the NO_x production channel from the 308 nm HNO_3 photolysis. This motivated us to revisit the nature of the NO_x production channel from the 308 nm HNO_3 photolysis due to its importance in understanding HONO formation in the troposphere.

In the work described in this paper, we directly measured absorption spectra of the NO_x product(s) in the 552−560 and 640−648 nm regions following 308 nm gas-phase photolysis of HNO_3 by using cavity ring-down spectroscopy.[32,33] Photolysis studies were conducted in the absence and in the presence of water vapor. A temporal absorption profile around 552 nm following HNO_3 photolysis was obtained. A survey study was also conducted in the near-UV region, where both HONO and NO_2 exhibit absorption. Discussions are presented concerning whether HONO formation is energetically feasible following actinic UV photolysis of a HNO_3/H_2O only system.

2. EXPERIMENTAL SECTION

The experimental setup is briefly described here. Details can be found elsewhere.[34−36] The output from a 308 nm excimer laser (Coherent; LPX 110i) is introduced into a stainless-steel reaction cell at a 15° angle, with the main cell axis through a side arm. The probe beam from a dye laser (Continuum, ND6000) pumped by a Nd:YAG laser (Continuum, Surelite II) is directed along the main optical axis of the cell, which is vacuum-sealed with a pair of high-reflectance cavity mirrors. Laser dyes used include Rhodamin 590, 4-dicyanomethylene-2-methyl-6-(*p*-dimethylaminostyryl)-4*H*-pyran (DCM), and pyridine 1 (LDS-698). The probe beam overlaps geometrically with the photolysis beam at the center of the cavity. The photolysis/probe laser overlap region can be conceptualized as a rectangular prism in which the prism's center coincides with that of the cell; its width and height are defined by those of the photolysis beam, and its length is defined by (beam width) × $(\tan 15°)^{-1}$, where 15° is the crossing angle between the pump and the probe laser beams. The length of the photolysis/probe laser overlap region is defined by (beam width) × $(\sin 15°)^{-1}$. A 12 mm wide × 6 mm tall rectangular aperture is placed in the photolysis beam path prior to the beam's entrance to the cell. For a 12 mm wide photolysis beam, the length of the photolysis/probe laser overlap region is about 4.6 cm. After the probe beam enters the cell through the front cavity mirror, its intensity decay inside the cavity is monitored with a photomultiplier tube (PMT) placed behind the back cavity mirror. The PMT output is amplified, digitized, and transferred to a computer. The decay curve is fitted to a single-exponential decay function, from which the ring-down time constant (τ) and the total loss (Γ) per round-trip pass are calculated. Spectra for HNO_3 and its photolysis product were recorded by scanning the wavelength of the probe beam in the 552−560 and 640−648 nm regions in the absence and in the presence of the photolysis beam. Potential HONO product following 308 nm photolysis of HNO_3 in the presence of H_2O was examined by probing absorptions at 342.0 and 343.5 nm (corresponding to the peak and valley of HONO absorption), both with and without photolysis pulses. A pulse/delay generator was used to vary the delay time between the firings of the photolysis and the probe lasers.

High-purity HNO_3 was prepared by vacuum distillation of a 3:2 mixture of sulfuric acid (98%; Mallinckrodt Baker) and nitric acid (70%; Mallinckrodt Baker) at 273 K; the distilled HNO_3 was collected into a trap cooled at ethanol/dry ice temperature (195 K).[37] At least four successive distillations were conducted to purify the HNO_3 sample. Extra distillation of the HNO_3 sample was done on the day of the experiment to further reduce NO_2 impurities. After the purification, we subsequently transferred HNO_3 into a clean bubbler and continued purging NO_2 by flowing N_2 carrier gas through the bubbler (held in ice−water bath) for about 20−25 min, followed by pumping the bubbler (held in ice−water bath) in the absence of N_2 flow for about 10−15 min. The NO_2 impurity in the purified HNO_3 vapor was determined to be about 0.02%, obtained by measuring NO_2 absorption *in situ* in the 552−560 nm region using cavity ring-down spectroscopy. Distilled water was drawn from a Barnstead nanopure ultrapure water system (Thermo Scientific, USA); the distilled water was evacuated at room temperature for 30 min to remove dissolved air.

The HNO_3 pressure inside the cell was monitored by using an MKS Baratron capacitance manometer (10 Torr full scale, measurement accuracy is about 10^{-4} Torr). The inner surfaces of the cell and the stainless steel joints on the gas transport lines were treated with halocarbon wax or grease (series 1500 or 25-5S; Halocarbon Products Corp.) to minimize decomposition of HNO_3 on surfaces. Although coating of the cell surfaces with halocarbon wax decreased the rate of decomposition of HNO_3, the NO_2 impurity in HNO_3 was found to increase with residence time in the cell on the time scale of several minutes. For a quantitative HNO_3 photolysis product study, an equivalent method of fast flow was used. In other words, HNO_3 was first evacuated in the bubbler, and then it was introduced into the cell. The photolysis and background measurements were carried out immediately after filling the cell with the fresh HNO_3 sample (the background and the photolysis measurements were done at time scales of less than 25 s in order to beat the background NO_2 increase), and afterward the HNO_3 sample was pumped out. We repeated this procedure for every experiment. Detailed methodology used in studying the photolysis of HNO_3/H_2O mixture is described in the Results and Discussion section. All experiments were carried out at an ambient temperature of 295 K.

DOI: 10.1021/acs.jpca.5b00951
J. Phys. Chem. A 2015, 119, 4907−4914

3. RESULTS AND DISCUSSION

3.1. Gas-Phase Photolysis of HNO_3 in the Absence of Water Vapor. *3.1.1. Nitric Acid and Photolysis Product Spectra in the 640−648 nm Region.* Shown in Figure 1 are

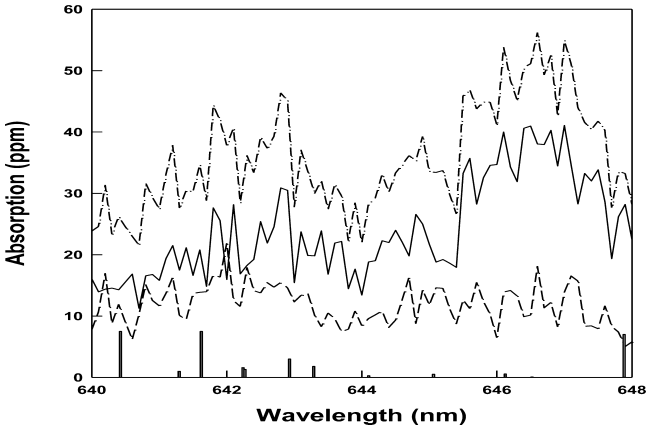

Figure 1. Cavity ring-down absorption spectra of 1.2 Torr HNO_3 in the 640−648 nm region, in the absence (solid line) and in the presence (dash-dot line) of 308 nm photolysis. The spectra were recorded at a wavelength interval of 0.1 nm. The difference spectrum is shown as a medium-dashed line. The bar graph shows literature[38] vibronic band origins and line intensities in electronically exited NO_2 ($^2B_2$).

nitric acid absorption spectra in the 640−648 nm region recorded by cavity ring-down spectroscopy, in the absence and in the presence of 308 nm photolysis pulses, and the difference spectrum. Also illustrated in Figure 1 are literature[38] vibronic band origins and line intensities in electronically excited $NO_2(^2B_2)$.

A comparison of the difference spectrum with literature NO_2* vibronic band origins and line intensities in the same wavelength region shows that NO_2* has a different spectral pattern compared with that of the HNO_3 photolysis product, suggesting that NO_2* is not formed from HNO_3 photolysis at 308 nm.

3.1.2. Nitric Acid and Photolysis Product Spectra in the 552−560 nm Region. Our previous study[29] showed that the 308 nm HNO_3 photolysis product displays absorption in the 552−560 nm region. Both NO_2 and NO_2* have broad visible absorptions;[39,40] 552−560 nm is at the longer-wavelength tail of the ground-state NO_2 absorption spectrum.[41−43] It is also the wavelength range at which NO_2* starts to exhibit absorption.[38,44−46] In our previous study, we monitored the decay of product absorption at 552.57 nm and obtained a decay time constant of 55 μs. The measured decay time constant, which was within the range of the literature decay lifetime of NO_2* of 55−90 μs, led us to suggest that NO_2* + OH is a predominant channel from the 308 nm photolysis of HNO_3. (The ground-state NO_2 was monitored at 352 nm. The total absorption of HNO_3 and the NO_2 impurity was on the order of thousands of ppm; transient ground-state NO_2 formation was not observed after the HNO_3 photolysis.) Yet, a direct comparison of the 308 nm HNO_3 photolysis product spectrum to that of literature NO_2* in the 640−648 nm region in the current study (Figure 1) suggests that NO_2* is not formed. So could the product spectrum in the 552−560 nm region come from the ground-state NO_2 generated by HNO_3 photolysis at 308 nm? Could NO_2 impurity in the HNO_3 sample have interfered with the decay profile measurement at 552.57 nm in the previous study? Could the NO_2 impurity in the sample be too high, such that NO_2 formed from the 308 nm HNO_3 photolysis was too small in comparison, which led to the conclusion that the ground-state NO_2 was not formed in the previous study? To address these questions, we prepared a high-purity HNO_3 sample and used an independent method to measure the NO_2 impurity concentration *in situ* at the time of the experiment.

To ensure high purity of the HNO_3 sample for the photolysis study, we always performed a redistillation of the HNO_3 sample on the day of the experiment in the current study. In the previous study,[29] we did not perform additional distillation on the day of the experiment. We later found that additional distillation on the day of the experiment significantly reduces the NO_2 impurity in the HNO_3 sample. Also, our previously reported[29] NO_2 impurity (<0.05%) was determined at the sample preparation and made at 448−452 nm. Knowing that NO_2 impurity in the sample varies with time and using absorption cross-section data for NO_2 in the 552−560 nm region obtained in this study, we directly determined the NO_2 impurity in the HNO_3 sample immediately before the photolysis experiment.

Shown in Figure 2 are cavity ring-down absorption spectra of 1.0 Torr HNO_3 vapor in the 552−560 nm region in the

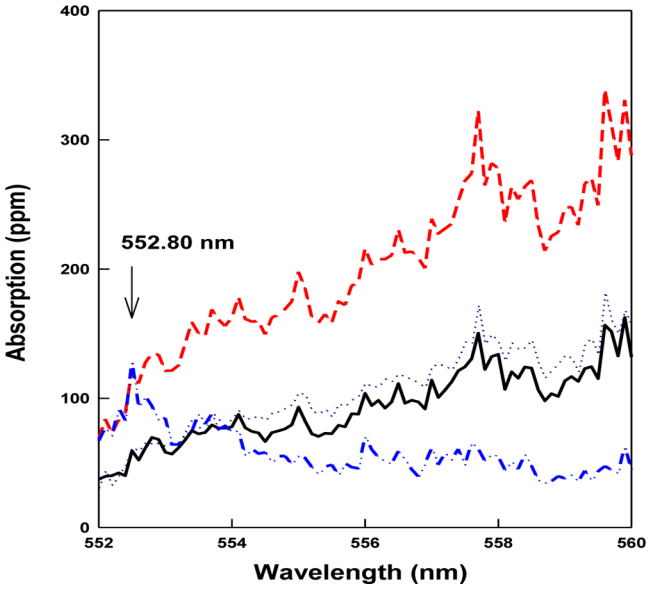

Figure 2. Cavity ring-down absorption spectra of 1.0 Torr HNO_3 vapor in the 552−560 nm region in the absence (solid line) and in the presence (dashed line) of photolysis at 308 nm. Both spectra were taken under closed cell conditions and at a wavelength interval of 0.1 nm. The difference spectrum (dotted line) for HNO_3 with and without photolysis is also included. Also shown for comparison is a cavity ring-down absorption spectrum (dash-dot-dot line) of a 1:98.3 NO_2:N_2 mixture at a NO_2 partial pressure of 0.33 mTorr.

absence (solid line) and in the presence (dashed line) of 308 nm photolysis. The plots showed that the abssorbance was increased after HNO_3 was photolyzed at 308 nm. The spectra were scanned from shorter wavelength to longer wavelengths, and during the spectral recording process (it took about 10 min to complete a spectral scan), the decomposition of HNO_3 contributed to the upward sloping of the recorded spectra. A close examination shows that the peaks and valleys of both

DOI: 10.1021/acs.jpca.5b00951
J. Phys. Chem. A 2015, 119, 4907−4914

spectra are matched to each other, suggesting that no new species were formed and the ground-state NO_2 is likely a product from the HNO_3 gas-phase photolysis. Also plotted in Figure 2 is an absorption spectrum of a 1:98.3 mixture of NO_2:N_2 with NO_2 partial pressure of 0.33 mTorr in the cell. A comparison of the NO_2 spectrum and that of the HNO_3 photolysis product provides clear experimental evidence that ground-state NO_2 is indeed a product from the HNO_3 photolysis. To understand the cause of time-resolved absorption at 552.57 nm from the HNO_3 photolysis in our previous study,[29] we tuned the cavity ring-down spectrometer to the product absorption maximum at 552.80 nm. (The probe laser system used in the previous study was replaced with a more accurate current probe laser system; there is slight difference in wavelength reading, but it is within the uncertainty of the instrument.) Transient round-trip absorptions from the HNO_3 photolysis at 0.5, 1.0, and 2.0 Torr pressures were measured as a function of delay time between the firing of the photolysis and the probe laser. We cannot decrease the HNO_3 pressure much lower than 0.5 Torr, as the product absorption in the 552−560 nm region decreases with decreasing HNO_3 pressure; we need to have a sufficient signal-to-noise ratio to prove the point. Illustrated in Figure 3 is a temporal absorption profile from the photolysis of 1.0 Torr HNO_3.

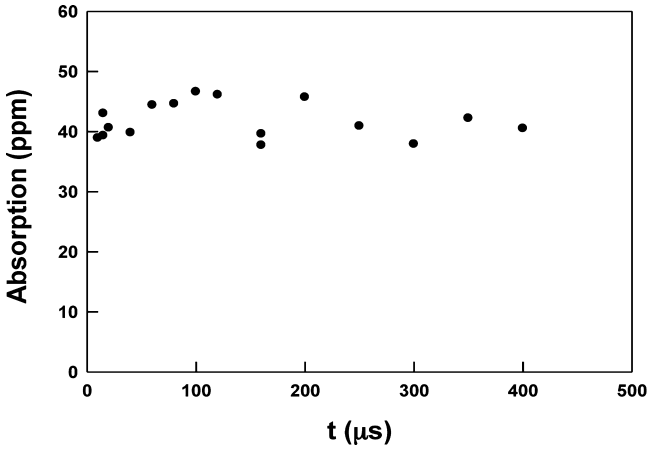

Figure 3. Round-trip absorption at 552.80 nm as a function of pump−probe laser delay time after 308 nm photolysis of 1.0 Torr HNO_3. Each absorption value is that from an accumulation of 10 photolysis pulses.

Consistency checks at 15 μs were performed at the beginning, in the middle, and at the end of the time dependence experiments. Absorptions at 552.80 nm from photolyzing 0.5, 1.0, or 2.0 Torr HNO_3 were found to be independent of the photolysis/probe laser delay time over the 10−400 μs range, within the experimental error. The lack of temporal dependence of the product absorption from the 308 nm photolysis of HNO_3 in the 0.5−2.0 Torr range, and the larger product absorption in the 552−560 nm region compared to that in the 640−648 nm region is consistent with the ground-state NO_2 (not the electronically excited NO_2) being a product from the 308 nm photolysis of HNO_3.

Reported decay lifetimes of NO_2* with NO_2 as a quencher are in the range of 30−100 μs as the NO_2 excitation wavelength is varied in the 398−600 nm range.[48−54] The long lifetime of NO_2* is postulated to arise from the vibrational energy mismatch between the vibronically excited NO_2 (i.e., NO_2*) and the ground-state NO_2;[55] thus, the vibrational-to-vibrational (V→V) energy transfer between NO_2* and NO_2 bath molecules is not that efficient. The quenching rate constant of NO_2* by NO_2 was found to decrease with decreasing photon energy used to excite NO_2 to NO_2*.[48] The rate constant for quenching of NO_2* by HNO_3 has not been previously reported. In the presence of a quencher such as 0.5−2.0 Torr HNO_3, the lifetime of the presumed NO_2* is expected to be shorter than the literature NO_2* decay lifetime of 30−100 μs. If NO_2* were indeed a predominant NO_x product formed from the 308 nm HNO_3 photolysis, we would expect to see absorption at 552.80 nm showing a prompt increase immediately after photolysis, and then decreasing quickly with delay time on a short time scale in Figure 3. But that is not the case in the current study. So why did our previous study[29] show time-resolved absorption in the 552−560 nm region? Was such time dependence real, or was it a spurious effect likely caused by the NO_2 impurity in the previous HNO_3 sample? In our earlier study,[29] the temporal absorption profile was determined by performing measurements at short photolysis/probe laser delay times first, and then at intermediate delay times, and subsequently at longer delay times. The NO_2 impurity in the HNO_3 bubbler decreased with increasing pumping-flow time, and the experiment was done from shorter delay time to longer delay time. This is equivalent to sampling more NO_2 absorption at a shorter delay time and less at a longer delay time. Interference from the NO_2 impurity could give this coincidental agreement between the HNO_3 photolysis product decay rate constant and the literature-reported decay rate constant of NO_2*. As mentioned earlier in this section, our previous study had a higher NO_2 impurity in the HNO_3 sample. In addition, no *in situ* measurement of the NO_2 impurity level was made during the photolysis experiments in the previous study. A constant NO_2 impurity level in HNO_3 was assumed in the slow-flow system in the previous study. Our current *in situ* measurement shows that the NO_2 impurity level in HNO_3 is not constant; it decreases with time in the slow-flow system. We also concluded that it is best to prepare the high-purity HNO_3 rather than to use this flow system to remove the NO_2 impurity in HNO_3. The latter depends on the delicate balance between the impurity NO_2 formation and removal rate. Given that the previous study had more NO_2 impurity in the HNO_3 sample, and that the impurity level could be variable and was not monitored in the experiment, the results of the current study should supersede those from our previous study.[29]

The ground-state NO_2 quantum yield from the HNO_3 photolysis at 308 nm was obtained from the ratio of the NO_2 concentration generated in the photolysis/probe laser overlap region per photolysis pulse to the absorbed photon density in the same region. Absorbed photolysis photon density in the pump/probe laser overlap region was derived from the difference between the transmitted photolysis beam energies entering (E_{in}) and leaving (E_{out}) that region, the individual photon energy (hc/λ) at the photolysis wavelength (λ), and the volume (v) of the overlap region. The photolysis beam energy entering or leaving the overlap region was calculated from the incident photolysis beam energy entering the cell (E_0), the HNO_3 absorption cross section (σ_{HNO_3}) at 308 nm, the HNO_3 concentration (n_{HNO_3}) in the cell, and the absorbing path length, by applying Beer's law:

$$E_{in} = E_0 \exp(-\sigma_{HNO_3} n_{HNO_3} l_1) \quad (4)$$

DOI: 10.1021/acs.jpca.5b00951
J. Phys. Chem. A 2015, 119, 4907−4914

$$E_{out} = E_0 \exp(-\sigma_{HNO_3} n_{HNO_3} l_2) \quad (5)$$

where l_1 represents the distance between the incident beam at the cell entrance and the initial position of the overlap region, and l_2 denotes the distance between the photolysis beam entrance and the end of the overlap region. E_0 was determined by a Joulemeter placed in front of the cell. The photolysis energy inside the cell was corrected for transmission loss at the front cell window and for reflection of the photolysis beam from the rear cell window. The incident photolysis fluence inside the cell was determined to be 0.04−0.05 J/cm^2. In light of low photolysis fluence, a multiphoton excitation process is unlikely. We previously obtained a HNO_3 absorption cross section of $(1.24 \pm 0.19) \times 10^{-21}$ cm^2/molecule at 308 nm using cavity ring-down spectroscopy.[29]

The NO_2 concentration generated from 308 nm photolysis of HNO_3 per photolysis pulse was acquired from measurements of the round-trip NO_2 absorption at 552.80 nm averaged over the number of photolysis pulses used. The NO_2 concentration resulting from HNO_3 photolysis at a given HNO_3 pressure can be obtained from the corresponding round-trip NO_2 absorption per photolysis pulse, the length of the photolysis/probe laser overlap region (l), and the absorption cross section of NO_2, σ_{NO_2}, using the equation $[NO_2]$ = Absorption/$(2\sigma_{NO_2} l)$. We directly measured the NO_2 absorption cross section at 552.80 nm to be $(1.34 \pm 0.05) \times 10^{-19}$ cm^2/molecule. Using the HNO_3 absorbed photon density and NO_2 absorption determined in this study, we obtain a NO_2 quantum yield of 1.1 ± 0.2 from the HNO_3 photolysis at 308 nm, independent of HNO_3 pressure (~Torr range).

3.2. 308 nm Gas-Phase Photolysis of HNO_3 in the Presence of Water Vapor. To understand the photolysis of the HNO_3/H_2O mixture at 308 nm, we first examined what happened to the cavity loss at 552.80 nm when H_2O was introduced into the cell. Cavity loss increased significantly after the water vapor was introduced into an evacuated reaction cell, previously exposed to HNO_3. This phenomenon suggested that the water vapor likely dispersed HNO_3 or NO_2 that was adsorbed on the cell wall. The back-filled water vapor was then pumped away along with HNO_3 that was adsorbed on the chamber wall. This process was repeated a number of times to condition the cell wall.

We noticed that it took a much longer time for the water vapor than for HNO_3 to reach equilibrium pressure inside the cell. In the experiment, H_2O was introduced into the cell first to allow it sufficient time to reach equilibrium pressure. During this time, HNO_3 was pumped in the bubbler. When the H_2O pressure reached the equilibrium inside the cell, the HNO_3 vapor was then admitted to the cell. The HNO_3/H_2O mixture background absorption was first determined, followed by prompt measurement of absorption of the 308 nm photolyzed mixture. In this way, the photolysis of the equilibrated HNO_3/H_2O mixture was studied. Presented in Figure 4 is a plot of absorption at 552.80 nm as a function of photolysis/probe laser delay time after 308 nm photolysis of mixtures containing 1.0 Torr HNO_3 and 0.2 Torr H_2O. Figure 4 shows that absorption at 552.80 nm is independent of delay time after the photolysis of the HNO_3/H_2O mixtures, suggesting that the HNO_3 photolysis product does not react with H_2O. If NO_2* were the predominant product formed from the 308 nm photolysis of the HNO_3 vapor, and if NO_2* underwent physical and/or chemical quenching by H_2O, we should expect absorption at 552.80 nm to decay with time. The lack of time-dependent

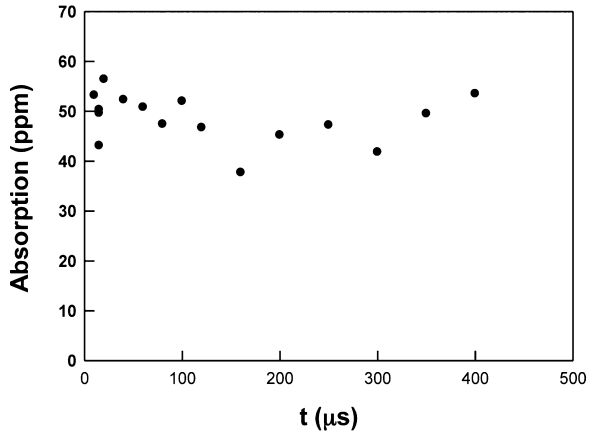

Figure 4. Round-trip absorption at 552.80 nm as a function of time after 308 nm photolysis of mixtures containing 1.0 Torr HNO_3/0.2 Torr H_2O.

absorption from the photolysis of mixtures containing 1.0 Torr HNO_3/0.2 Torr H_2O or 1.1 Torr HNO_3/0.5 Torr H_2O is consistent with ground-state NO_2 being formed from the 308 nm photolysis of the HNO_3/H_2O mixture.

To investigate whether HONO was formed from the 308 nm photolysis of HNO_3/H_2O mixture, we also tuned the wavelengths of the ring-down probe beam to those at 342.0 and 343.5 nm, where literature peak and valley of HONO absorption are located.[56−60] A brief survey study showed that absorptions at 342.0 and 343.5 nm are comparable in size but lack temporal dependence following the 308 nm photolysis of HNO_3/H_2O mixtures. This result suggests that HONO is not formed from the 308 nm photolysis of a HNO_3/H_2O mixture. Since ground-state NO_2 is produced from the 308 nm photolysis of HNO_3, it is not surprising that we did not observe HONO formation at <1 ms after the 308 nm photolysis of the HNO_3/H_2O mixture. The reaction of ground-state NO_2 with H_2O ($2NO_2 + H_2O + M = HNO_3 + HONO + M$) occurs slowly through a heterogeneous process, with a rate constant of ~2.4×10^{-23} cm^3 molecule^{-1} s^{-1}.[61]

3.3. Comparison with Literature Studies and Atmospheric Implications. Both the photolysis product absorption spectrum and the lack of dependence of absorption on photolysis/probe laser delay time in the 552−560 nm region indicate that the NO_x produced from the 308 nm photolysis of HNO_3 is NO_2 in the ground electronic state. Our observation is consistent with those from the HNO_3 photodissociation dynamics studies.[18,27] On the basis of thermodynamic analysis and a literature report,[7] one might argue for the formation of some NO_2* from the 308 nm photolysis of HNO_3. But if we take the symmetry, barrier, and adiabatic state correlation into the consideration, our experimental observation can be fully explained. *Ab initio* calculation showed that the ground state and two lowest energy excited states of HNO_3 are $1^1A'$, $1^1A''$, and $2^1A''$.[7] The energy differences between these two electronically excited states and the ground state are 3.40 and 4.54 eV, respectively.[7,62] Once a HNO_3 molecule absorbs a 308 nm photon, it can be excited into the first electronically excited $1^1A''$ state due to the fact that the absorption band is broad and the vertical excitation energy is 3.73 eV. In terms of electronic structure, the transition essentially involves excitation of an electron from a nonbonding NO_2 molecular orbital to a NO_2 π^* antibonding orbital in HNO_3, with symmetry $a' \rightarrow a''$ (C_s). This HNO_3 $1^1A''$ quantum state is correlated with X^2A_1 in

DOI: 10.1021/acs.jpca.5b00951
J. Phys. Chem. A 2015, 119, 4907−4914

NO_2,[7,18] which is the ground electronic state of the NO_2 molecule. On the other hand, 308 nm light is not energetic enough to access $2^1A''$ of HNO_3 (4.54 eV);[7,61] this $2^1A''$ state is correlated with 1^2B_2, which is the first electronically excited state of NO_2. The correlation diagram is shown in Figure 5.

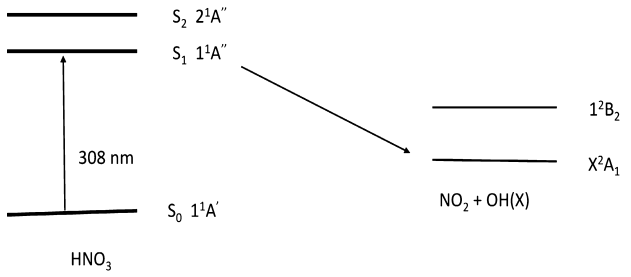

Figure 5. Sketch of the HNO_3 photodissociation energy level diagram based upon ref 18.

Photodissociation of HNO_3 at $2^1A''$ is governed by both symmetry and barrier height. Despite the broad HNO_3 absorption, the energy barrier is the limiting step to form NO_2*. This supports well our experimental observation that only the ground-state NO_2 is observed from the 308 nm photolysis of HNO_3.

Our experimental results are consistent with the ground-state NO_2 being the only NO_x product formed from the 308 nm HNO_3 photolysis. Energetically, the electronically excited NO_2 1^2B_2 is accessible via HNO_3 $1^1A''$, but it is symmetry-forbidden (Figure 5). We cannot totally exclude a minor NO_2* channel (e.g., less than a few percent) formed through a hypothetical, non-adiabatic HNO_3 photodissociation pathway. For example, if there were non-adiabatic interaction between $1^1A''$ and higher electronically excited state(s) of HNO_3, or if the geometry of HNO_3 (NO_2 angle) were changed in such a way that the symmetry-forbidden pathway became allowed, the HNO_3 photolysis product might have some characteristics of electronically excited NO_2 1^2B_2. Nonetheless, we expect this hypothetical non-adiabatic HNO_3 photodissociation channel to be of minor importance.

In this paper, we have re-examined the NO_x product channel from the 308 nm photolysis of HNO_3 in the gas phase; we found ground-state NO_2 to be the experimentally observed NO_x product from this photodissociation process, with a near-unit quantum yield. The ground-state NO_2 may also be expected to be the NO_x product formed from adsorbed HNO_3 photolysis in the daytime troposphere. As the near-UV absorption cross sections of surface-adsorbed HNO_3 are 2−3 orders of magnitude larger than those in the gas phase,[47,63] photolysis of adsorbed HNO_3 molecules by sunlight is an efficient renoxification process and an important source of OH radicals. However, photolysis of an adsorbed HNO_3-only system by actinic UV radiation is not expected to be significant for tropospheric HONO formation, as the solar photon energy in the troposphere is likely not energetic enough to form the HONO product.

AUTHOR INFORMATION

Corresponding Author

*Tel: 518-474-6846; fax: 518-473-2895; e-mail: lzhu@albany.edu.

Present Address

†L.H.: California Air Resources Board, Sacramento, CA

Notes

The authors declare no competing financial interest.

ACKNOWLEDGMENTS

Discussions with Profs. J. Robert Huber, G. A. Segal, and John R. Barker are acknowledged. We are grateful for the support provided by the National Science Foundation under grant no. AGS-0969985.

REFERENCES

(1) Kleffmann, J.; Gavriloaiei, T.; Hofzumahaus, A.; Holland, F.; Koppmann, R.; Rupp, L.; Schlosser, E.; Siese, M.; Wahner, A. Daytime Formation of Nitrous Acid: A Major Source of OH Radicals in a Forest. *Geophys. Res. Lett.* **2005**, *32*, L05818 DOI: 10.1029/2005GL022524.

(2) Sarwar, G.; Roselle, S. J.; Mathur, R.; Appel, W.; Dennis, R. L.; Vogel, B. A Comparison of CMAQ HONO Predictions with Observations from the Northeast Oxidant and Particle Study. *Atmos. Environ.* **2008**, *42*, 5760−5770.

(3) Zhou, X.; Gao, H.; He, Y.; Huang, G.; Bertman, S. B.; Civerolo, K.; Schwab, J. Nitric Acid Photolysis on Surfaces in Low-NO_x Environments: Significant Atmospheric Implications. *Geophys. Res. Lett.* **2003**, *30*, 2217 DOI: 10.1029/2003GL018620.

(4) Zhou, X.; Civerolo, K.; Dai, H.; Huang, G.; Schwab, J. J.; Demerjian, K. L. Summertime Nitrous Acid Chemistry in the Atmospheric Boundary Layer at a Rural Site in New York State. *J. Geophys. Res.* **2002**, *107*, 4590 DOI: 10.1029/2001JD001539.

(5) Zhou, X. L.; He, Y.; Huang, G.; Thornberry, T. D.; Carroll, M. A.; Bertman, S. B. Photochemical Production of Nitrous Acid on Glass Sample Manifold Surface. *Geophys. Res. Lett.* **2002**, *29*, 1681 DOI: 10.1029/2002GL015080.

(6) Lide, D. R. *CRC Handbook of Chemistry and Physics*; CRC Press: Boca Raton, FL, 2008.

(7) Huber, J. R. Photochemistry of Molecules Relevant to the Atmosphere: Photodissociation of Nitric Acid in the Gas Phase. *ChemPhysChem* **2004**, *5*, 1663−1669.

(8) Bai, Y. Y.; Segal, G. A. Features of the Electronic Potential Energy Surfaces of Nitric Acid below 7 eV. *J. Chem. Phys.* **1990**, *92*, 7479−7483.

(9) Bérces, T.; Förgeteg, S. Kinetics of Photolysis of Nitric Acid Vapour. Part 1. Direct Photolysis at Low Conversion. *Trans. Faraday Soc.* **1970**, *66*, 633−639.

(10) Johnston, H. S.; Chang, S.-G.; Whitten, G. Photolysis of Nitric Acid Vapor. *J. Phys. Chem.* **1974**, *78*, 1−7.

(11) Jolly, G. S.; Singleton, D. L.; McKenney, D. J.; Paraskevopoulos, G. Laser Photolysis of HNO_3 at 222 nm: Direct Determination of the Primary Quantum Yield of OH. *J. Chem. Phys.* **1986**, *84*, 6662−6667.

(12) Kenner, R. D.; Rohrer, F.; Papenbrock, Th.; Stuhl, F. Excitation Mechanism for OH(A) in the ArF Excimer Laser Photolysis of Nitric Acid. *J. Phys. Chem.* **1986**, *90*, 1294−1299.

(13) Jacobs, A.; Kleinermanns, K.; Kuge, H.; Wolfrum, J. OH($X\ ^2\Pi$) State Distribution from HNO_3 and H_2O_2 Photodissociation at 193 nm. *J. Chem. Phys.* **1983**, *79*, 3162−3163.

(14) Turnipseed, A. A.; Vaghjiani, G. L.; Thompson, J. E.; Ravishankara, A. R. Photodissociation of HNO_3 at 193, 222, and 248 nm: Products and Quantum Yields. *J. Chem. Phys.* **1992**, *96*, 5887−5895.

(15) Margitan, J. J.; Watson, R. T. Kinetics of the Reaction of the Hydroxyl Radicals with Nitric Acid. *J. Phys. Chem.* **1982**, *86*, 3819−3824.

(16) Schiffman, A.; Nelson, D. D., Jr.; Nesbitt, D. J. Quantum Yields for OH Production from 193 and 248 nm Photolysis of HNO_3 and H_2O_2. *J. Chem. Phys.* **1993**, *98*, 6935−6946.

(17) Felder, P.; Yang, X.; Huber, J. R. Photodissociation of Nitric Acid in a Cold Molecular Beam at 193 nm. *Chem. Phys. Lett.* **1993**, *215*, 221−227.

(18) Myers, T. L.; Forde, N. R.; Hu, B.; Kitchen, D. C.; Butler, L. J. The Influence of Local Electronic Character and Nonadiabaticity in

DOI: 10.1021/acs.jpca.5b00951
J. Phys. Chem. A 2015, 119, 4907−4914

the Photodissociation of Nitric Acid at 193 nm. *J. Chem. Phys.* **1997**, *107*, 5361−5373.
(19) Li, Q.; Carter, R. T.; Huber, J. R. The Photodissociation Dynamics of Nitric Acid Studied at 193 nm by LIF and TEMPI-TOF Methods. *Chem. Phys. Lett.* **2001**, *334*, 39−46.
(20) Leu, G.-H.; Hwang, C.-W.; Chen, I.-C. Distribution of Internal States of OH ($X\ ^2\Pi$) from Photodissociation of Nitric Acid. *Chem. Phys. Lett.* **1996**, *257*, 481−486.
(21) Schlütter, J.; Kleinermanns, K. OH($X\ ^2\Pi$) State Distribution from HNO_3 Photodissociation at 212.5 and 270 nm. *Chem. Phys. Lett.* **1992**, *192*, 94−98.
(22) Assenmacher, F.; Gutmann, M.; Noack, F.; Stert, V.; Radloff, W. Femtosecond Photodissociation Dynamics of HNO_3 after Excitation of the S_3-State at 200 nm. *Appl. Phys. B: Laser Opt.* **2000**, *71*, 385−390.
(23) Graña, A. M.; Lee, T. J.; Head-Gordon, M. Ab Initio Calculations of Singlet and Triplet Excited States of Chlorine Nitrate and Nitric Acid. *J. Phys. Chem.* **1995**, *99*, 3493−3502.
(24) McCabe, D. C.; Brown, S. S.; Gilles, M. K.; Talukdar, R. K.; Smith, I. W. M.; Ravishankara, A. R. Kinetics of the Removal of OH(ν=1) and OD(ν=1) by HNO_3 and DNO_3 from 253 to 383 K. *J. Phys. Chem. A* **2003**, *107*, 7762−7769.
(25) Sinha, A.; Vander Wal, R. L.; Crim, F. F. State-Resolved Unimolecular Reactions: The Vibrational Overtone Initiated Decomposition of Nitric Acid. *J. Chem. Phys.* **1990**, *92*, 401−410.
(26) Krisch, M. J.; Reid, M. C.; McCunn, L. R.; Butler, L. J.; Shu, J. Photofragment Translational Spectroscopy of Nitric Acid at 248 nm with VUV Photoionization Detection of Products. *Chem. Phys. Lett.* **2004**, *397*, 21−25.
(27) August, J.; Brouard, M.; Simons, J. P. Photofragment Vector Correlations and Dissociation Dynamics in $HONO_2$. *J. Chem. Soc. Faraday Trans. 2* **1988**, *84*, 587−598.
(28) Riffault, V.; Gierczak, T.; Burkholder, J. B.; Ravishankara, A. R. Quantum Yields for OH Production in the Dissociation of HNO_3 at 248 and 308 nm and H_2O_2 at 308 and 320 nm. *Phys. Chem. Chem. Phys.* **2006**, *8*, 1079−1085.
(29) Zhu, C.; Xiang, B.; Chu, L. T.; Zhu, L. 308 nm Photolysis of Nitric Acid in the Gas Phase, on Aluminum Surfaces and on Ice Films. *J. Phys. Chem. A* **2010**, *114*, 2561−2568.
(30) Delon, A.; Jost, R. Laser Induced Dispersed Fluorescence Spectra of Jet Cooled NO_2: The Complete Set of Vibrational Levels Up to 10000 cm^{-1} and the Onset of the X^2A_1-$\tilde{A}^2B_2$ Vibronic Interaction. *J. Chem. Phys.* **1991**, *95*, 5686−5700.
(31) Leonardi, E.; Petrongolo, C. *Ab Initio* Study of NO_2. VI. Vibrational and Vibronic Coupling in the $X^2A_1/\tilde{A}^2B_2$ Conical Intersection up to 16000 cm^{-1}. *J. Chem. Phys.* **1997**, *106*, 10066−10071.
(32) O'Keefe, A.; Deacon, D. A. G. Cavity Ring-Down Optical Spectrometer for Absorption Measurements Using Pulsed Laser Sources. *Rev. Sci. Instrum.* **1988**, *59*, 2544−2551.
(33) O'Keefe, A.; Scherer, J. J.; Cooksy, A. L.; Sheeks, R.; Heath, J.; Saykally, R. J. Cavity Ring Down Dye Laser Spectroscopy of Jet-Cooled Metal Clusters: Cu_2 and Cu_3. *Chem. Phys. Lett.* **1990**, *172*, 214−218.
(34) Zhu, L.; Johnston, G. Kinetics and Products of the Reaction of the Vinoxy Radical with O_2. *J. Phys. Chem.* **1995**, *99*, 15114−15119.
(35) Zhu, L.; Ding, C.-F. Temperature Dependence of the Near UV Absorption Spectra and Photolysis Products of Ethyl Nitrate. *Chem. Phys. Lett.* **1997**, *265*, 177−184.
(36) Zhu, L.; Kellis, D. Temperature Dependence of the UV Absorption Cross Sections and Photodissociation Products of C_3-C_5 Alkyl Nitrates. *Chem. Phys. Lett.* **1997**, *278*, 41−48.
(37) Rattigan, O.; Lutman, E.; Jones, R. L.; Cox, R. A.; Clemitshaw, K.; Williams, J. Temperature-Dependent Absorption Cross-Sections of Gaseous Nitric-Acid and Methyl Nitrate. *J. Photochem. Photobiol., A* **1992**, *66*, 313−326.
(38) Persch, G.; Mehdizadeh, E.; Demtröder, W.; Zimmermann, Th.; Köppel, H.; Cederbaum, L. S. Vibronic Level Density of Excited NO_2-States and Its Statistical Analysis. *Ber. Bunsenges. Phys. Chem.* **1988**, *92*, 312−318.
(39) Hsu, D. K.; Monts, D. L.; Zare, R. N. *Spectral Atlas of Nitrogen Dioxide*; Academic Press: New York, 1978.
(40) Smalley, R. E.; Wharton, L.; Levy, D. H. The Fluorescence Excitation Spectrum of Rotationally Cooled NO_2. *J. Chem. Phys.* **1975**, *63*, 4977−4989.
(41) Davidson, J. A.; Cantrell, C. A.; McDaniel, A. H.; Shetter, R. E.; Madronich, S.; Calvert, J. G. Visible-Ultraviolet Absorption Cross Sections for NO_2 as a Function of Temperature. *J. Geophys. Res.—Atmos.* **1988**, *93* (D6), 7105−7112.
(42) Schneider, W.; Moortgat, G. K.; Tyndall, G. S.; Burrows, J. P. Absorption Cross-Sections of NO_2 in the UV and Visible Region (200−700 nm) at 298 K. *J. Photochem. Photobiol., A: Chem.* **1987**, *40*, 195−217.
(43) Vandaele, A. C.; Hermans, C.; Simon, P. C.; Carleer, M.; Colin, R.; Fally, S.; Merienne, M. F.; Jenouvrier, A.; Coquart, B. Measurements of the NO_2 Absorption Cross-Section from 42,000 cm^{-1} to 10,000 cm^{-1} (238−1000 nm) at 220 and 294 K. *J. Quant. Spectrosc. Radiat. Transfer* **1998**, *59*, 171−184.
(44) Georges, R.; Delon, A.; Jost, R. The Visible Excitation Spectrum of Jet Cooled NO_2: The Chaotic Behavior of a Set of $^2B_2$ Vibronic Levels. *J. Chem. Phys.* **1995**, *103*, 1732−1747.
(45) Delon, A.; Georges, R.; Jost, R. The Visible Excitation Spectrum of Jet Cooled NO_2: Statistical Analysis of Rovibronic Interactions. *J. Chem. Phys.* **1995**, *103*, 7740−7772.
(46) Delon, A.; Jost, R. NO_2 Jet Cooled Visible Excitation Spectrum: Vibronic Chaos Induced by the X^2A_1-$\tilde{A}^2B_2$ Interaction. *J. Chem. Phys.* **1991**, *95*, 5701−5718.
(47) Du, J.; Zhu, L. Quantification of the Absorption Cross Sections of Surface-Adsorbed Nitric Acid in the 335−365 nm Region by Brewster Angle Cavity Ring-Down Spectroscopy. *Chem. Phys. Lett.* **2011**, *511*, 213−218.
(48) Myers, G. H.; Silver, D. M.; Kaufman, F. Quenching of NO_2 Fluorescence. *J. Chem. Phys.* **1966**, *44*, 718−723.
(49) Haas, Y.; Houston, P. L.; Clark, J. H.; Moore, C. B.; Rosen, H.; Robrish, P. Long-lived K_a = 0, $^2B_1$ States of NO_2: A Direct Measurement Using a Tunable Dye Laser. *J. Chem. Phys.* **1975**, *63*, 4195−4197.
(50) Paech, F.; Schmiedl, R.; Demtröder, W. Collision Free Lifetimes of Excited NO_2 Under Very High Resolution. *J. Chem. Phys.* **1975**, *63*, 4369−4378.
(51) Stevens, C. G.; Swagel, M. W.; Wallace, R.; Zare, R. N. Analysis of Polyatomic Spectra Using Tunable Laser-Induced Fluorescence: Applications to the NO_2 Visible Band System. *Chem. Phys. Lett.* **1973**, *18*, 465−469.
(52) Schwartz, S. E.; Johnston, H. S. Kinetics of Nitrogen Dioxide Fluorescence. *J. Chem. Phys.* **1969**, *51*, 1286−1302.
(53) Donnelly, V. M.; Kaufman, F. Fluorescence Lifetime Studies of NO_2. I. Excitation of the Perturbed $^2B_2$ State Near 600 nm. *J. Chem. Phys.* **1977**, *66*, 4100−4110.
(54) Chen, C. H.; Kramer, S. D.; Clark, D. W.; Payne, M. G. Studies of Lifetimes of Rotationally Cooled NO_2 Using Time-Resolved Fluorescence Excitation Spectra. *Chem. Phys. Lett.* **1979**, *65*, 419−424.
(55) Douglas, A. E. Anomalously Long Radiative Lifetimes of Molecular Excited States. *J. Chem. Phys.* **1966**, *45*, 1007−1015.
(56) Bongartz, A.; Kames, J.; Welter, F.; Schurath, U. Near-UV Absorption Cross Sections and Trans/Cis Equilibrium of Nitrous Acid. *J. Phys. Chem.* **1991**, *95*, 1076−1082.
(57) Pagsberg, P.; Bjergbakke, E.; Ratajczak, E.; Sillesen, A. Kinetics of the Gas Phase Reaction OH + NO(+ M) → HONO(+ M) and the Determination of the UV Absorption Cross Sections of HONO. *Chem. Phys. Lett.* **1997**, *272*, 383−390.
(58) Stockwell, W. R.; Calvert, J. G. The Near Ultraviolet Absorption Spectrum of Gaseous HONO and N_2O_3. *J. Photochem.* **1978**, *8*, 193−203.
(59) Stutz, J.; Kim, E. S.; Platt, U.; Bruno, P.; Perrino, C.; Febo, A. UV-Visible Absorption Cross Sections of Nitrous Acid. *J. Geophys. Res.* **2000**, *105*, 14585−14592.

DOI: 10.1021/acs.jpca.5b00951
J. Phys. Chem. A 2015, 119, 4907−4914

(60) Vasudev, R. Absorption Spectrum and Solar Photodissociation of Gaseous Nitrous Acid in the Actinic Wavelength Region. *Geophys. Res. Lett.* **1990**, *17*, 2153−2155.
(61) Ramazan, K. A.; Syomin, D.; Finlayson-Pitts, B. J. The Photochemical Production of HONO During the Heterogeneous Hydrolysis of NO_2. *Phys. Chem. Chem. Phys.* **2004**, *6*, 3836−3843.
(62) Nonella, M.; Suter, H. U.; Huber, J. R. An ab Initio and Dynamics Study of the Photodissociation of Nitric Acid HNO_3. *Chem. Phys. Lett.* **2010**, *487*, 28−31.
(63) Zhu, C.; Xiang, B.; Zhu, L.; Cole, R. Determination of Absorption Cross Sections of Surface-Adsorbed HNO_3 in the 290−330 nm Region by Brewster Angle Cavity Ring-Down Spectroscopy. *Chem. Phys. Lett.* **2008**, *458*, 373−377.

DOI: 10.1021/acs.jpca.5b00951
J. Phys. Chem. A 2015, 119, 4907−4914